

Crystal Structure of Unliganded Phosphofructokinase from *Escherichia coli*

Wojciech R. Rypniewski† and Philip R. Evans

Medical Research Council Laboratory of Molecular Biology
Hills Road, Cambridge CB2 2QH, England

(Received 26 October 1988, and in revised form 21 February 1989)

In an attempt to characterize the mechanism of co-operativity in the allosteric enzyme phosphofructokinase from *Escherichia coli*, crystals were grown in the absence of activating ligands. The crystal structure was determined to a resolution of 2.4 Å by the method of molecular replacement, using the known structure of the liganded active state as a starting model, and has been refined to a crystallographic *R*-factor of 0.168 for all data. Although the crystallization solution would be expected to contain the enzyme in its inactive conformation, with a low affinity for the co-operative substrate fructose 6-phosphate, the structure in these crystals does not show the change in quaternary structure seen in the inactive form of the *Bacillus stearothermophilus* enzyme (previously determined at low resolution), nor does it show any substantial change in the fructose 6-phosphate site from the structure seen in the liganded form. Compared to the liganded form, there are considerable changes around the allosteric effector site, including the disordering of the last 19 residues of the chain. It seems likely that the observed conformation corresponds an active unliganded form, in which the absence of ligand in the effector site induces structural changes that spread through much of the subunit, but cause only minor changes in the active site. It is not clear why the crystals should contain the enzyme in a high-affinity conformation, which presumably represents only a small fraction of the molecules in the crystallizing solution. However, this structure does identify the conformational changes involved in binding of the allosteric effectors.

1. Introduction

The allosteric enzyme phosphofructokinase (PFKase‡, EC 2.7.1.11) is one of the key control enzymes in glycolysis. It catalyses the phosphorylation of fructose 6-phosphate (Fru-6-*P*) to fructose-1,6-bisphosphate (Fru-1,6-*P*₂), in the presence of ATP. The PFKase from *Escherichia coli* has been studied extensively (Blangy *et al.*, 1968) but phosphofructokinases from *Bacillus stearothermophilus*, *Thermus aquaticus* (Hengartner & Harris, 1975) and *Thermus X-1* (Cass & Stellwagen, 1975) show similar kinetics. The enzyme shows co-operative kinetics with respect to the substrate Fru-6-*P*, but not with respect to the other substrate, ATP, allosteric activation by ADP and allosteric inhibition by phosphoenolpyruvate (PEP). The kinetics of the

allosteric bacterial phosphofructokinases may be described in terms of a concerted two-state model (Monod *et al.*, 1965; Rubin & Changeux, 1966), which assumes an equilibrium between two conformational states, R and T, differing in their affinity for the co-operative substrate Fru-6-*P*, and for the allosteric effectors. The less active state, the T-state, is predominant in the absence of ligands. Allosteric activators (ADP and GDP) and inhibitor PEP alter the equilibrium by binding preferentially to the R-state and the T-state, respectively (heterotropic interactions). Fru-6-*P* also alters the equilibrium by binding more strongly to the R-state (homotropic interactions). To a first approximation, the enzyme behaves as a “K system”, which means that the two states differ in the binding affinity (*K*_m) for Fru-6-*P* but not in their catalytic rates (*V*_{max} and *k*_{cat}). However, the kinetics show some departure from the simplest model, in that activation by GDP increases *V*_{max} by 20% over the value achieved by Fru-6-*P* activation alone (S. A. Berger, unpublished results). This suggests that the active conformation induced by binding Fru-6-*P* is further altered by binding GDP (or ADP).

† Present address: Institute for Enzyme Research, University of Wisconsin, 1710 University Avenue, Madison, Wisconsin 53705, U.S.A.

‡ Abbreviations used: PFKase, phosphofructokinase; Fru-6-*P*, fructose 6-phosphate; Fru-1,6-*P*₂, fructose-1,6-bisphosphate; PEP, phosphoenolpyruvate; PEG, polyethylene glycol.

The structure of the active conformation has been determined for *B. stearothermophilus* PFKase in its complex with Fru-6-P and ADP/Mg²⁺ (Evans & Hudson, 1979; Evans *et al.*, 1981), and for the 54% homologous *E. coli* PFKase with its reaction products Fru-1,6-P₂ and ADP/Mg²⁺ (Shirakihara & Evans, 1988). The structure is summarized in Figure 1. Two distinct changes in the enzyme conformation have been observed by comparing different crystal structures. Firstly, the crystal structure of the active form of *E. coli* PFKase shows two different conformations of subunits (Shirakihara & Evans, 1988). The differences lie within the large domain and consist mainly of a shift of helices 4a, 4 and 5 towards the Fru-6-P binding site (see Fig. 1(b) and (c)). The shift results in the closing of the cleft between the domains, bringing the ATP molecule about 1 to 1.5 Å (1 Å = 0.1 nm) nearer to Fru-6-P. The two conformations will be referred to later as "open" (chain Y) and "closed" (chain X). This conformational change is remote from the subunit interfaces, and involves the non-co-operative substrate ATP, so is presumably important for catalysis, not for the control properties of the enzyme. Secondly, the change to the inactive conformation (T-state) has been observed at 7 Å resolution in the crystal structure of the inhibited form of the PFKase from *B. stearothermophilus*, in crystals grown with the PEP analogue 2-phosphoglycolate (Evans *et al.*, 1986). This structure determination has recently been extended to 2.5 Å resolution (T. Schirmer, unpublished results), essentially confirming the earlier result. Compared to the active state, the tetramer is twisted about the *p*-axis by 8°, resulting in a partial closing of the Fru-6-P site.

In an attempt to obtain more detailed information about the low-affinity conformation (T-state) of *E. coli* PFKase, crystals were grown in the absence of activators and in the presence of inhibitors. This paper describes the structure at 2.4 Å resolution of such a crystal form, grown under conditions where the T-state conformation would be expected, and compares it with the structure of the active form (R-state). Although the structures differ around the effector site, their similarity in the active site suggest that the observed conformation corresponds to a high-affinity form.

2. Materials and Methods

(a) Crystallization

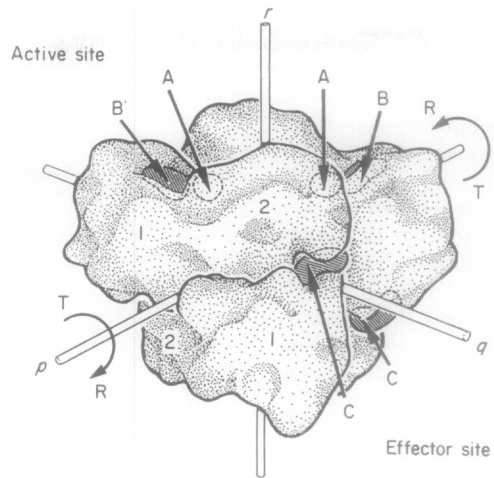
Phosphofructokinase was prepared from cultures of *E. coli* containing an overproducing plasmid, as described by Shirakihara & Evans (1988). A dozen crystal forms of phosphofructokinase were grown in the absence of ligands or in the presence of a non-physiological inhibitor 2-phosphoglycolate. The most suitable crystal form for high-resolution diffraction was obtained from solution containing 10 mg of the enzyme/ml, 14% (w/v) polyethylene glycol (PEG) 6000, 1.0 to 1.1 M-NaCl, 50 mM-Tris·HCl (pH 7.7 to 7.9). Crystals grew in both the presence and absence of 10 mM-2-phosphoglycolate. For reproducible growth, it was necessary to seed with a diluted suspension of ground-up crystals. The polyethylene glycol solution was treated with Amberlite ion-exchange resin to remove ionic impurities (e.g. phosphate). The crystals were grown in small glass vials containing 50 to 100 μl of solution. They grew as needles 2 to 3 mm long and 0.2 to 0.3 mm thick. X-ray photographs showed that the crystals diffracted to 2.3 Å resolution and belonged to space group *C2*. The cell parameters were determined accurately by repeatedly scanning several strong high-angle reflections on a 4-circle diffractometer, at various configurations of the goniostat to eliminate errors in the angle zeroes. The final values were: $a = 177.02$ Å, $b = 66.40$ Å, $c = 153.97$ Å, $\beta = 118.83^\circ$. From the cell volume, the unit cell was estimated to contain 4 tetramers ($V_M = 2.90$ Å³/dalton, within the observed range of 1.7 Å³/dalton to 3.5 Å³/dalton; Matthews, 1968). The crystals were stabilized by transfer to a solution containing 20% (w/v) PEG 6000, 1.0 M-NaCl, 50 mM-Tris·HCl (pH 7.7). The crystals became disordered after about a month at room temperature.

(b) Data collection and processing

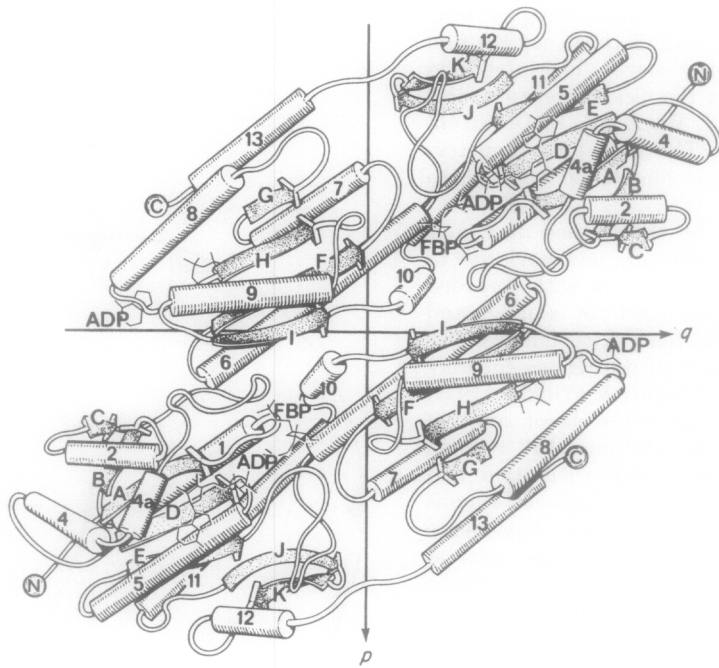
Low-resolution data were collected to 7 Å resolution from a single crystal on a 4-circle diffractometer with an ω scan. Crystals were cooled to -4°C. The profile-fitting method of Oatley & French (1982) was used to get more accurate values for weak reflections. Absorption correction was done according to North *et al.* (1968). The R_{sym}^\dagger for the intensities was 0.043. High-resolution data were

$\dagger R_{\text{sym}}, R_{\text{merge}} = \Sigma |I_i - \langle I \rangle| / \Sigma \langle I \rangle$, where I_i is an individual measurement, and $\langle I \rangle$ is the weighted mean intensity for this reflection. For R_{sym} , the summations are over equivalent reflections on the same film (or within a diffractometer data set). For R_{merge} , the summations are over all data.

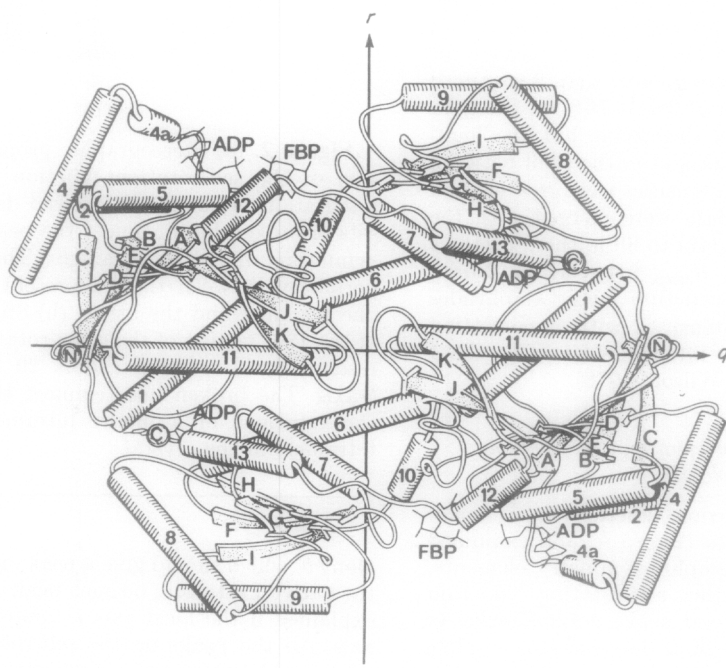
Figure 1. Schematic views of the structure of phosphofructokinase. The enzyme is a tetramer of identical subunits arranged around 3 orthogonal dyad axes in such a way that each subunit is in contact with only 2 other subunits. Each subunit is clearly divided into 2 domains, each consisting of a β -sheet sandwiched between α -helices. Three binding sites, designated A, B and C, have been identified. Sites A and B form the active site and bind Fru-6-P (or Fru-1,6-P₂), and ATP/Mg²⁺ or ADP/Mg²⁺, respectively. Site C is the allosteric effector site, which binds both activators (ADP or GDP) and the inhibitor PEP. Both the Fru-6-P and the effector sites lie between 2 subunits: the Fru-6-P sites across the *r*-interface and the effector sites across the *p*-interface. On the other hand, the non-co-operative substrate ATP binds entirely within 1 subunit. (a) Schematic view of the PFKase tetramer, showing the elongated subunits divided into 2 domains: the large domain is labelled 1, the small domain 2. The molecular dyad axes are labelled *p*, *q*, *r*. The ligand binding sites are marked. The overall direction of the shift between R- and T-states is shown as a twist around the *p*-axis (see Evans *et al.*, 1986). (b) R-state structure: view of the 2 subunits related by the *r*-axis. The other 2 subunits are behind. Helices are represented by cylinders, β -sheet strands by arrows. The active site is shown with the reaction products Fru-1,6-P₂ (FBP) and ADP, the effector site with the activator ADP (Evans & Shirakihara, 1988). (c) R-state structure: view of the 2 subunits related by the *p*-axis. The other 2 subunits are behind.



(a)



(b)



(c)

Fig. 1.

collected on beam line 7.2 at the Daresbury Synchrotron Radiation Source, using CEA Reflex film, at a wavelength of 1.488 Å. The crystals were cooled to -8°C . The oscillation range varied from 1.1° to 1.7° , depending on the crystal orientation and the axis of mounting; exposure times were between 30 s and 1 min per degree depending on the intensity of the beam. Because of the elongated shape of the crystals it was possible to collect data from 3 to 4 parts of the crystal by moving it along the spindle axis. One carousel-full (8 film-packs) was collected from each part of the crystal. In all, data were used from 7 crystals on 191 film packs: 161 with the b -axis mounted along the spindle axis and 30 with the crystal mounted about an axis perpendicular to the spindle, to record the cusp region. The films were digitised on an Optronics densitometer with the scanning raster size of $50\ \mu\text{m}$. The densitometer was previously calibrated using a test-wedge, made by exposing, for various times, a CEA film with an americium/copper X-ray source. The integrated intensities were measured from the files of digitized films using program MOSFLM (A. J. Wonacott, S. Dockerell, P. Brick & A. G. W. Leslie). The R_{sym} for symmetry-equivalent reflections on the same film varied from 0.03 to 0.09.

Films were scaled together by the method of Fox & Holmes (1966), including a temperature factor relative to the best film. Initially, only reflections with recorded fractions greater than 1.2 were used for scaling, and adjacent partially recorded reflections were summed: this gave $R_{\text{merge}} = 0.114$. Three rounds of postrefinement were performed using the method of Schutt & Winkler (1977, also Winkler *et al.*, 1979), to improve the classification of reflections as either fully or partially recorded, refining cell dimensions for each crystal, and orientation and crystal mosaicity for each film pack. In the first 2 rounds isotropic beam divergence was assumed. The dependence of the intensity of a partial reflection on the angular fraction (the rocking curve) was modelled by a hyperbolic tangent function. In the third round of postrefinement an anisotropic beam divergence was assumed. After rejecting a few films with unreasonably large relative temperature factors (< -10) the final R_{merge} was 0.103. The merged data, to $2.4\ \text{\AA}$ resolution, contained 388,304 observations, which reduced to 59,481 unique reflections. Unmatched partials with fraction greater than 0.4 were scaled for inclusion; 67% of the data were greater than 3 standard deviations. Up to a resolution of $2.6\ \text{\AA}$, 76% of the data were greater than 3 standard deviations but the high-resolution reflections were weak and in the shell between $2.6\ \text{\AA}$ and $2.4\ \text{\AA}$ only 34% of intensities were greater than 3 standard deviations. The data were merged with the low-resolution diffractometer data to fill in the reflections that were too strong on film. R_{merge} between the 2 data sets was 0.057. Finally, the structure factor amplitudes were calculated from the intensities with a correction applied to weak and negative intensities based on the *a priori* distribution (French & Wilson, 1978).

(c) *Determination of the orientation and positions of the molecules*

Native Patterson and rotation functions were calculated using low-resolution data (7 to 5 Å) and examined to identify the non-crystallographic symmetry elements. The $\kappa = 180^{\circ}$ section of the self-rotation function (Crowther, 1972) showed several peaks perpendicular to the b -axis, which requires a peak at the b -axis to complete a 222 set (Fig. 2(a)). This implied that one of the molecular dyad axes was parallel to the crystallographic dyad

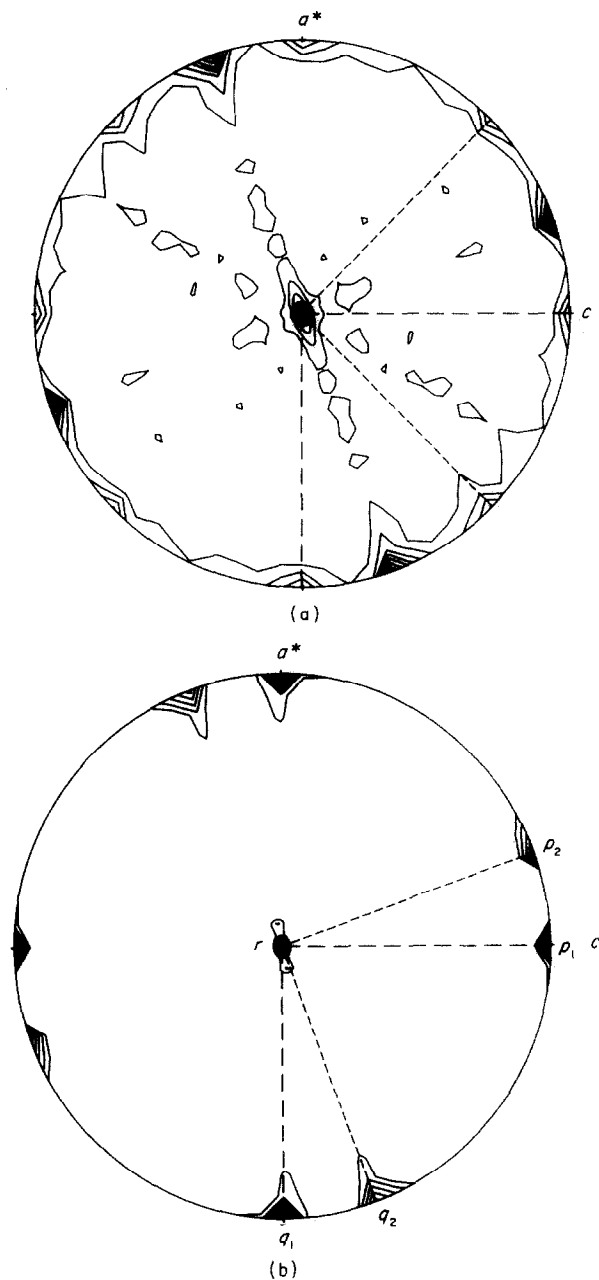


Figure 2. (a) Stereographic projection of the 180° section of the self-rotation function (7 to 5 Å resolution, integration radius 29 Å), viewed down the b -axis. The 2 sets of broken lines connect the peaks related by the 222 symmetry of the 2 tetramers. The large peaks on the periphery between these represent the vectors between one tetramer and the other. (b) Stereographic projection of the 180° section of the cross-rotation function (7 to 5 Å resolution, integration radius 29 Å), viewed down the b -axis. The broken lines connect the peaks representing the rotations of a model tetramer to the 2 different tetramers in the crystal.

along b , which should give a peak on the Harker section of the native Patterson; no such peak was found. This can be explained if the local axis is coincident with the crystal axis. All the peaks on the self-rotation function can be explained by 2 tetramers each sitting on different crystallographic dyad axes, with the asymmetric unit containing

two half-tetramers. Fig. 2(a) shows the 2 orthogonal sets of peaks for the different tetramers at 45° to each other. Between them there are strong peaks relating the 2 molecules. These peaks are at double weight as there are twice as many vectors involved in superimposing 2 tetramers as in superimposing 2 half-tetramers. The non-crystallographic symmetry also leads to mirror planes in the diffraction pattern, which can be seen in the precession photograph of the $h0l$ zone.

The cross-rotation function calculated using the known R -state model, with individual atomic temperature factors (Shirakihara & Evans, 1988), confirmed this arrangement and showed which molecular axes (pqr) correspond to the non-crystallographic axes. Fig. 2(b) shows the 180° rotation section of the cross-rotation function showing that the model tetramer can be superimposed on the 2 tetramers in this crystal form by a rotation of 180° about c (half-way between 0° and 45°).

The relative position along y of the 2 tetramers was found by a translational R -factor search (Nixon & North, 1976) using data to 3 Å resolution. The search involved moving 1 tetramer relative to the other, since the overall origin is not fixed in space group $C2$. It was also possible to determine the orientation of the 2 tetramers a little more accurately by repeating the calculation for slightly different orientations. At 0.696 the R -factor dropped to 0.44 from an average of 0.50, for the 2 tetramers at -1.5° and 43.5° to the c -axis (Fig. 3).

In summary, a rather unusual packing arrangement was revealed: alternating, centred layers of PFK tetramers pack with the molecules in different layers rotated to each other by about 45° . Such arrangements of oligomeric proteins expressing crystallographic symmetry in different ways are rare (e.g. see Buehner *et al.*, 1982; Tanaka *et al.*, 1984).

(d) Rigid body refinement

The initial positional refinement of the PFKase molecules in the unit cell was done by treating various fragments of the molecules as rigid bodies, using the

program CORELS (Sussman *et al.*, 1977; Herzberg & Sussman, 1983). The co-ordinates of the R -state structure (Shirakihara & Evans, 1988) were used for the starting model. Two dimers were put in the positions and orientations determined from the rotation and translation searches. The first few cycles of CORELS were run with each subunit constrained to move as a rigid body, with a single temperature factor. The temperature factor was fixed and set to 20 in the first cycle and was allowed to vary thereafter. The first 3 cycles used low-resolution data from 15 Å to 7 Å. In the next 3 cycles the resolution was increased to 6 Å. The R -factor decreased from the initial value of 0.46 to 0.42. The rotations and translations were averaged between subunits and applied to the starting model co-ordinates. A further 13 cycles were performed with each subunit divided into 2 domains linked together by peptide bonds. The resolution was gradually increased to 4 Å. The final R -factor was 0.39. The overall changes in the model from the starting R -state model were rather small, with rotations of 1 to 2° and shifts of about 1 Å. No clear trends were apparent between the different subunits, but the refinement has clearly resulted in a moderate improvement in the model, as judged by the R -factor.

(e) Restrained least-squares refinement

Further refinement of the atomic co-ordinates and temperature factors was done using the method of restrained least-squares refinement (Konnert, 1976; Konnert & Hendrickson, 1980), with the X-ray component calculated using the program Deriv written by Jack (Jack & Levitt, 1978). All calculations were done in space group $C2_1$, which is equivalent to $C2$ with a translation of a $1/4a$ along the x -axis, so that the existing fast Fourier transform routines for space group $P2_1$ could be used. Fig. 4 shows the progress of the refinement. Diffraction data to the maximum resolution (2.4 Å) were used, but the low-resolution reflections (<10 Å) were excluded at this stage. The geometric restraints used are listed in Table 1. A shift factor of 0.55 was applied to calculated shifts in positions and temperature factors to give a

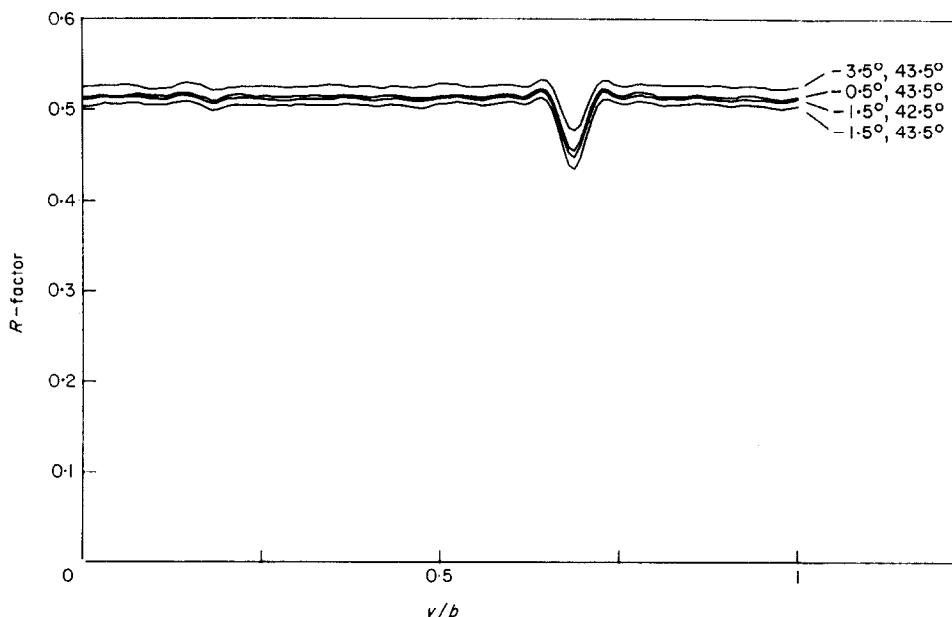


Figure 3. R -factor as a function of the relative translation along y between the 2 tetramers on different crystallographic dyads. Each line is for a different combination of rotations of the 2 tetramers about the b -axis.

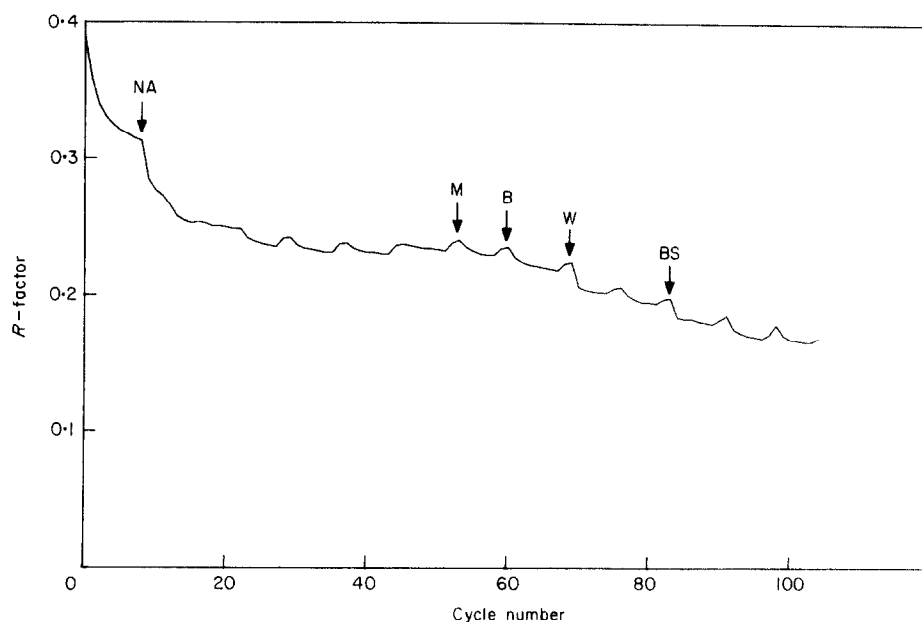


Figure 4. Progress of the refinement: plot of R -factor ($\Sigma||F_o| - |F_c||/\Sigma|F_o|$) against the cycle number of the least-squares refinement. Initially, the calculated gradients were averaged between the 4 independent subunits. The point labelled NA indicates where the averaging was terminated. M marks the point where molecular averaging was performed. At B the restraints on temperature factors were relaxed as described in text. Addition of ordered water molecules to the model began at W. At BS, a solvent continuum was included in the model by putting constant density in the solvent space. The spikes indicate cycles with tighter geometric constraints to regularize the structure prior to manual rebuilding.

reasonable rate of convergence while allowing for the diagonal approximation in the X-ray part of the normal matrix. In the first 8 cycles the calculated gradients were averaged for the 4 independent subunits to increase the radius of convergence in the initial stages of the refinement. The R -factor dropped from the initial value of 0.389 to 0.313.

Further refinement was done without averaging. Typically 5 to 7 cycles of refinement were followed by 2 regularizing cycles with the relative weight of structure factor component to the normal matrix reduced from 0.4 to 0.2, to achieve better stereochemistry at the cost of poorer fit with the diffraction data. The effect of regularizing on the R -factor can be seen as "bumps" on Fig. 4. The model was then adjusted manually from comparison with maps calculated using coefficients $2|F_o| - |F_c|$ and $|F_o| - |F_c|$ with calculated phases, using the program FRODO (Jones, 1978). From the first inspection it became clear that no major rebuilding of the model was necessary although several side-chains were clearly misplaced. The differences were consistent for all 4 crystallographically independent subunits and gave rise to clear negative and positive peaks on the $|F_o| - |F_c|$ map. This sensitivity in detecting misplaced residues, together with the absence of prominent features on the difference map elsewhere, suggested that the model was correct, at least in its well-defined parts. Some regions, generally on the surface of the molecule, were weakly defined or altogether absent. Residues that could not be seen included the N-terminal methionine and the last 20 residues of the C terminus. In general, the parts of the structure that were absent on the map or ambiguous were excluded from further refinement. These regions were inspected periodically to see if they became visible. If a side-chain could be made to fit the density in more than one way (Leu, Glu, Lys, Arg) the most sterically favourable conformation was chosen. Close inspection of the maps led to a modification of the amino acid sequence, determined from the

nucleotide sequence, with an insertion of Arg before Gly93 and change of Asn92 to Lys (see Shirakihara & Evans, 1988, for the corrected sequence). After about 50 cycles of refinement and a few rounds of rebuilding the R -factor

Table 1
Geometric parameters for the least-squares refinement and the values from the final model

	Target value	Final value
Distances (Å)		
Bond length (1-2 neighbour)	0.02	0.012
Angle-related distance (1-3 neighbour)	0.04	0.046
Interplanar distance (1-4 neighbour)	0.05	0.049
Planar groups (Å)	0.02	0.010
Chiral volumes (Å ³)	0.15	0.150
Non-bonded contacts (Å)		
Single torsion	0.50	0.198
Multiple torsion	0.50	0.283
Possible hydrogen bond	0.50	0.218
Torsion angles (°)		
Planar (e.g. peptide ω)	3	2.0
Staggered (e.g. aliphatic χ)	15	21.1
Transverse (e.g. aromatic χ_2)	20	25.4
Thermal factors (Å ²)		
Main-chain bond (nearest neighbour)	3.0	3.14
Main-chain angle (next nearest neighbour)	5.0	5.00
Side-chain bond (nearest neighbour)	3.0	4.06
Side-chain angle (next nearest neighbour)	5.0	6.59

The target value is the inverse square root of the least squares weight for each type of parameter. The final values are the root-mean-square deviations from ideal values (Konnert & Hendrickson, 1981).

had fallen to 0.24 but the C-terminal region was still absent. Some density could be seen in one of the subunits but it was far from clear how the C terminus could fit into it. At this stage electron density averaging was performed to improve, if possible, the quality of the map, particularly in that region.

(f) Molecular averaging

The method of electron density averaging was used as implemented in programme suite SKEWPLANES by G. Bricogne (1976). The symmetry relating the 4 independent subunits is improper, i.e. it does not form a point group. In this case, with 2 molecules in arbitrary orientations, at least 2 distinct envelopes are required, 1 for each tetramer, or 4 envelopes, each enclosing 1 crystallographically independent subunit. The latter option was chosen as being computationally simpler. As the C-terminal region lies on the surface of the subunit care had to be taken not to leave it outside the molecular envelope. To construct the envelope, electron density maps were calculated for each subunit with a large temperature factor ($= 40 \text{ \AA}^2$), with the C terminus in the same conformation as in the R-state. The non-zero regions were then flagged with their subunit number, smoothed to remove isolated zeroes and merged together. Transformations to relate each subunit to the others were calculated from the current co-ordinates, with each pair of subunits related by a dyad in the x - z plane and perpendicular to the y -axis. In the first 2 cycles of averaging the R -factor calculated with structure factors derived from the averaged map decreased from 0.242 to 0.197. Afterwards it started to increase and in cycle 8 it reached 0.265. It is a little difficult to explain this behaviour: it seems that some errors accumulated to overcome the initial improvement in phases. There are 2 major sources of error, other than those arising from the crystallographically independent subunits not being identical: one arises from inaccurate determination of the inter-subunit transformations, the other results from inaccurate definition of the molecular boundaries. Since the subunits are in contact, this problem could be particularly serious as one envelope could invade the space of the neighbouring subunit. An electron density map was calculated using phases from cycle 2 (the lowest R -factor). The map appeared unchanged although some minor adjustments were made to the model. The C terminus was still absent, reinforcing the view that it was disordered. Although the molecular averaging did not result in a significant improvement of the model, it reinforced our confidence in its correctness.

(g) Inclusion of ordered and disordered solvent

Many water molecules were clearly visible on both the $2|F_o| - |F_c|$ and $|F_o| - |F_c|$ maps. These were included in the model, especially if they lay within the hydrogen bonding distance of O or N atoms. Care was taken not to put water molecules into density representing an alternative conformation of a side-chain. No water molecules were placed in the region of the C terminus in case any missing residues became interpretable at some later time. The effect on the refinement was considerable: after the inclusion of the first 152 water molecules the R -factor decreased from 0.225 to 0.206. Water molecules that refined to a temperature factor of $B > 50 \text{ \AA}^2$ were eliminated.

Disordered solvent was approximated by a constant density in the solvent space. The method used was as described by Phillips (1980), Fermi *et al.* (1984) and Shirakihara & Evans (1988). The resolution limits could

then be extended to include the very low-order terms ($> 10 \text{ \AA}$). The final values for solvent scattering ρ_s was 0.34 e/\AA^3 and the solvent smoothing temperature factor B_{solv} was 52 \AA^2 .

3. Results

(a) The final model and crystal packing

The least-squares refinement was terminated when the R -factor reached 0.168. The different subunits in the final model were labelled A, B, C and D, with A and B belonging to one tetramer and C and D to the other. A total of 347 water molecules were also included. Most of the model fitted the density well, with reasonable geometry as summarized in Table 1. Some side-chains were disordered: these lay on the surface of the molecule or, significantly, in the binding sites. The last 19 residues (301 to 319) were disordered except in chain D where residues up to 304 could be located. Some density could be seen for the C-terminal region in chain D, but no satisfactory fit could be made.

Figure 5 shows the arrangement of molecules in the crystal. Layers of $(AB)_2$ tetramers in the x - y plane are interleaved with parallel layers of $(CD)_2$ tetramers. Within each layer, tetramers are related by the crystallographic C-centering operation $(x+1/2, y+1/2, z)$. Each tetramer fits into gaps between tetramers in the adjacent layers.

There are four regions of contacts between tetramers in the crystal.

(1) Contact between the A and C subunits involves N-terminal Met0A and Met115C[†] at the end of α -5. The two side-chains are antiparallel, about 3 \AA apart. This explains why the N terminus in chain A is ordered, as distinct from the other three subunits. The nearby loop between α -11 and β -J of chain A is in contact with α -4 of chain C. There are two hydrogen bonds: between O of Ala277A, through a water molecule, to O of Glu79C, and between OH of Tyr279A and O ϵ of Glu87C.

(2) Contact between B and D involves again the loop between α -5 and β -J from chain B and region near the C terminus of chain D. There are two hydrogen bonds: between O of Gly278B and N of Lys304D and between OH of Tyr279B and O of Asp298D. This explains why in chain D four more residues (301 to 304) were ordered at the C terminus.

(3) and (4) The two remaining contacts are very similar and result from the stacking of molecules along the y -axis. Thus A is in contact with B of the neighbouring tetramer and C is similarly in contact with D. The contacts are related by a non-crystallographic dyad, and involve helices α -9 packing parallel to each other. The most prominent is the interaction between the imidazole rings of His232. Being common to all subunits, this could be a major stabilizing interaction in the crystal and could explain why the crystal growth is rather sensitive to

[†] Residues are numbered from 0 to 319. Met115C means residue number 115 in chain C.

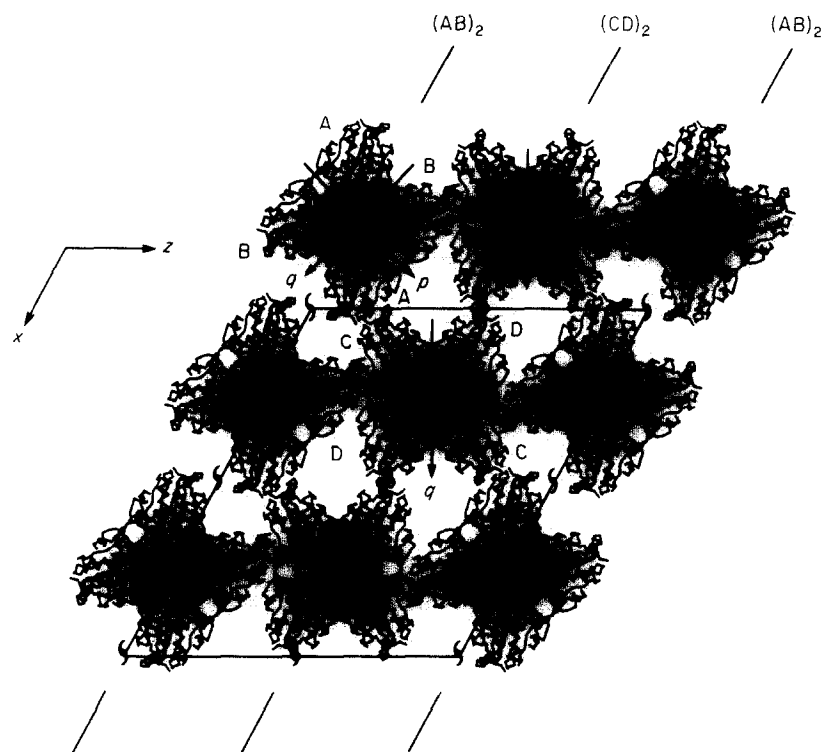


Figure 5. The packing of molecules in the crystal cell, viewed along the crystallographic y -axis. Each type of tetramer $(AB)_2$ and $(CD)_2$ is arranged in layers in the x - z plane, each sitting on a crystallographic dyad axis. The molecular axes are labelled p and q , with r along y .

pH. The imidazole rings could only stack if they had no net charge, which is consistent with the high pH range 7.7 to 7.9 within which the crystals grow. These similar interactions between the different tetramers may also explain their similar conformations.

(b) *Comparison between the four unliganded subunits*

For comparison of the subunits, the pairs of subunits were superimposed by a dyad axis constrained to pass through the perpendicular to the crystallographic dyad axes. This gave the orientations of the two tetramers as 43.84° and -1.32° (angle between p and z), and their separation along the y -axis of 20.87 \AA or $0.31b$. The co-ordinates of each subunit could then be transformed to a "molecular frame", with axes pqr along the dyads. Root-mean-square deviations are calculated between the subunits superimposed on the dyad axes, including the two different PFKase subunits of the liganded R-state (here denoted X for the closed chain, Y for the open chain; Shirakihara & Evans, 1988). From the results shown in Table 2 it can be seen that the four unliganded subunits fit quite well to each other with a better internal agreement than between X and Y. Chains A and B are the most similar and D is the most different from the other three. It can also be seen that the unliganded structures are more like the open (Y) liganded subunit than the closed (X) subunit. The internal agreement between the crystallographically independent subunits sets the

upper limit of the random error in co-ordinates. The actual errors are smaller when the effects of different crystallographic environments are taken into account.

The structures of the four independent subunits are closely similar: the differences in co-ordinates of

Table 2
Overall differences between subunits

		B	C	D	X	Y
A	All atoms	0.74	0.88	0.98	1.54	1.34
	Main chain	0.39	0.52	0.58	1.10	0.84
	Side-chains	1.00	1.15	1.29	1.91	1.73
B		—	0.84	0.93	1.53	1.27
			0.53	0.57	1.15	0.83
			1.08	1.22	1.87	1.62
C			—	0.97	1.60	1.36
				0.64	1.13	0.84
				1.24	1.99	1.78
D				—	1.61	1.34
					1.16	0.82
					1.99	1.74
X					—	1.02
						0.78
						1.23

Values are root-mean-square deviations (\AA) between subunits. Subunits were superimposed by aligning the molecular (pqr) frames. X and Y refer to closed and open subunits of the liganded R-state (Shirakihara & Evans, 1988).

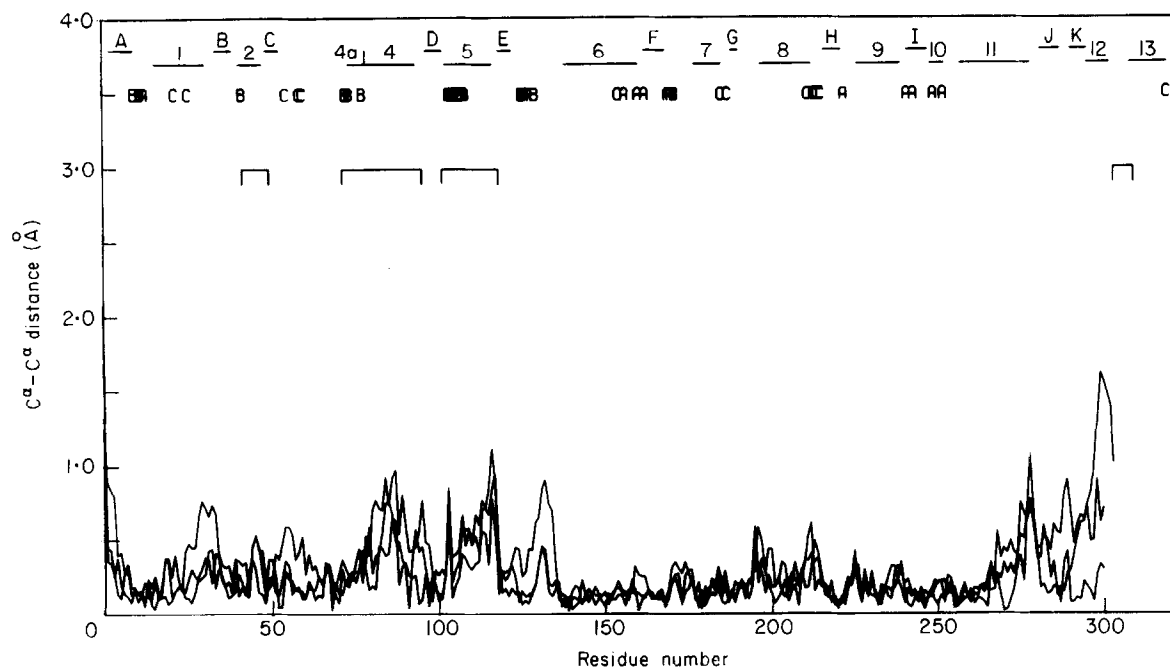


Figure 6. Differences in co-ordinates of α -carbons between the 4 independent subunits of the unliganded structure, superimposed on the molecular dyads. The plot shows the difference between subunit A and subunits B, C and D. The different subunits are closely similar (cf. liganded structures in Fig. 7). The differences reflect the random error in co-ordinates and the effect of the different crystallographic environment of the subunits. The small domain (residues 140 to 260) shows less variation than the larger domain except in helix α -13, at the C terminus, which is disordered. In this, and the following Figures, up to Fig. 11, the α -helices (1 to 13) and the strands of the β -sheets (A to K) are indicated on top of the plot. The position of the residues of the binding sites A, B and C are also indicated, as are the 4 main regions of difference between the open and closed liganded subunits.

α -carbons plotted along the chain in Figure 6 are generally smaller than between the two structures of the liganded enzyme (Fig. 7). The temperature

factors show a greater variation, as shown in Figure 8: the most conspicuous differences are in subunit D, near the C terminus and in chain C

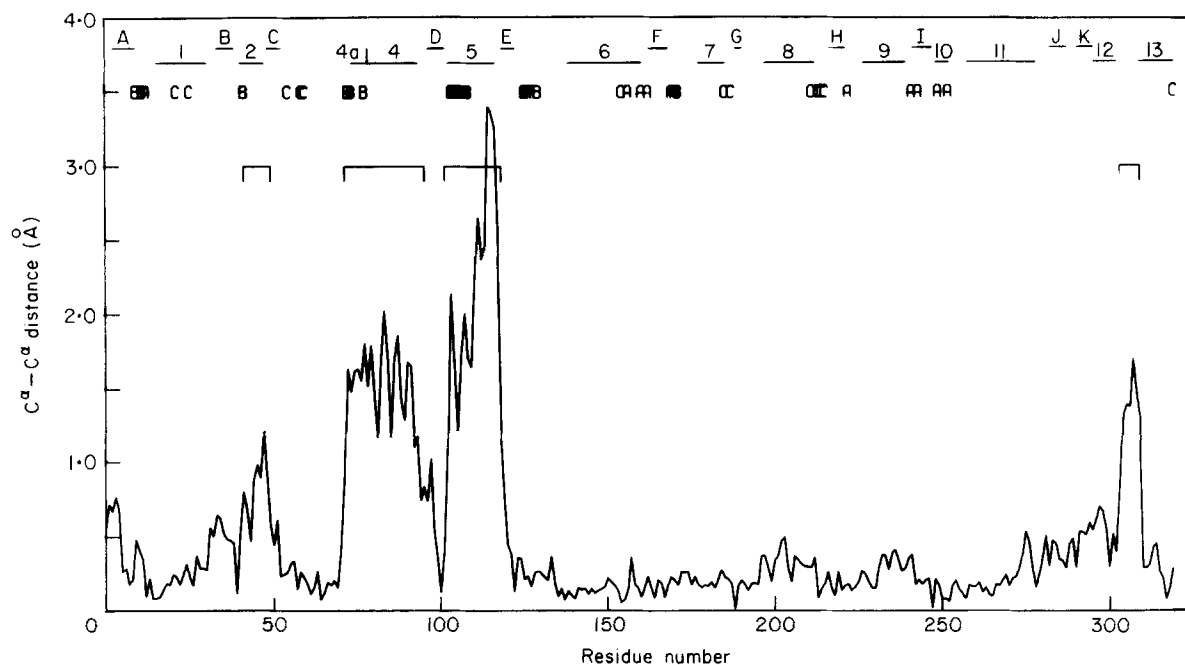


Figure 7. Differences in co-ordinates of α -carbons between the 2 independent subunits of the liganded R-state structure: open subunit (Y) and closed (X). Large differences of 2 to 3 Å can be seen in helices α -4 and α -5. The motion brings the 2 domains closer together in the closed structure. The region around residue 305 is poorly defined in both subunits.

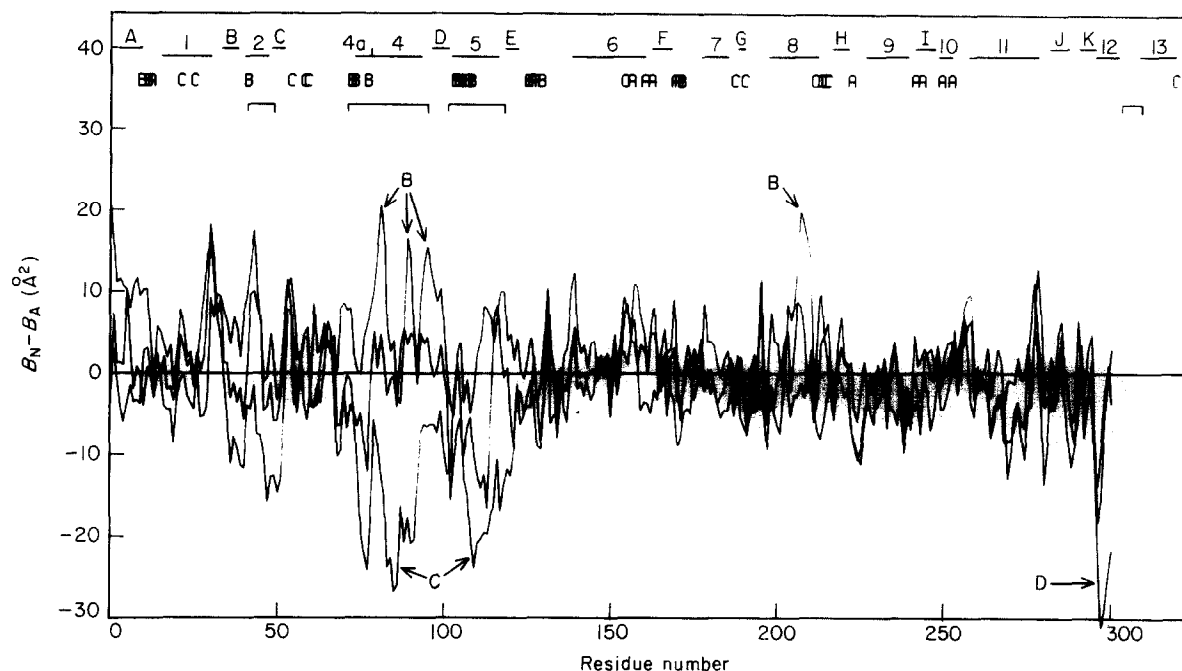


Figure 8. Differences in temperature factors between subunit A (B_A) and subunits B, C and D of the unliganded structure (B_N), calculated using temperature factors of the main-chain atoms averaged over each residue. The largest differences correspond to regions of intermolecular contacts.

between residues 75 and 120. Both of these correspond to regions of intermolecular contacts. Figures 6 and 7 illustrate both the magnitude and the random error and the extent to which the crystal environment can perturb the structure.

(c) *Comparison between non-liganded and liganded structures*

The rigidity (Table 4) and the relative movements (Table 5) of the secondary structure elements were analysed between one of the unliganded subunits

(B) and the two liganded subunits X and Y, using a program written by Arthur Lesk. The elements of secondary structure, α -helices and β -sheets, were identified from their hydrogen-bonding patterns (Table 3); [3] is not a proper α -helix, just a short helix-like segment without regular hydrogen bonding; 4a and 10 are 3_{10} helices. Helix 13 is at the C terminus, which is disordered in the unliganded

Table 3
Secondary structure elements as determined from hydrogen bonding

α -Helices	Residue range	β -Strands	Residue range
1	15-30	A	2-9
2	40-47	B	33-38
[3]	54-57	C	48-52
4a	73-78		
4	78-93	D	95-101
5	102-116	E	119-124
6†	138-161	F†	163-168
7†	174-185	G†	188-190
8†	197-213	H†	216-222
9†	226-239	I†	241-245
10†	249-253		
11	257-277	J	282-287
		K	290-294
12	296-300		
(13)	303-319		

† Secondary structure elements which form the smaller domain. Helix 13 is disordered in the unliganded structure.

Table 4
Rigidity of secondary structure elements

Elements of chain B	r.m.s. difference (Å) for fitting to chains:	
	Y	X
β -Sheets:		
A,B,C,D,E,J,K,F,G,H,I	0.29	0.33
	0.27	0.26
α -Helices:		
1	0.19	0.18
2	0.18	0.24
[3]	0.23	0.29
4	0.29	0.42
5	0.33	0.40
6	0.25	0.27
7	0.20	0.24
8	0.39	0.40
9	0.26	0.26
[10]	0.12	0.13
11	0.28	0.27
12	0.43	0.35
All atoms	0.58	0.69

Each secondary structure element (main chain only) for the unliganded chain B was fitted separately to the equivalent element in the liganded (Y, open, X, closed) structure, to show any conformational changes within the structural element. r.m.s., root-mean-square.

Table 5
Structural changes between liganded and unliganded forms

	Liganded chain			
	Y Translation (Å)	Y Rotation (°)	X Translation (Å)	X Rotation (°)
Superimposed on <i>pqr</i> axes				
Change for all atoms	0.25	1.4	0.45	2.0
<i>Large domain</i>				
Superimposed on sheet (A,B,C,D,E,J,K)				
Change for helix:				
1	0.09	0.4	0.23	1.6
2	0.15	2.0	0.55	4.3
[3]	0.41	2.5	0.36	1.0
4	0.15	2.5	0.80	5.4
5	0.28	2.8	1.40	5.5
11	0.16	0.3	0.22	1.7
12	1.28	27.4	1.88	22.5
Sheet (F,G,H,I)	0.86	1.3	0.96	2.0
<i>Small domain</i>				
Superimposed on sheet (F,G,H,I)				
Change for helix:				
6	0.27	2.0	0.22	1.4
7	0.27	1.8	0.17	3.4
8	1.30	9.4	1.23	9.0
9	0.33	5.0	0.33	3.8
[10]	0.30	1.3	0.32	1.1

Relative shifts of secondary structure elements (main chain only) between liganded (Y, open; X, closed) and unliganded (chain B) subunits. For the comparison of the whole subunit, the structures were superimposed on the molecular frame (*pqr*). For the comparisons within the domains, the subunits were superimposed on the β -sheets, and the shifts of the surrounding helices analysed.

structure. The elements of secondary structure are preserved rather well and to a first approximation can be considered to be rigid bodies (Table 4). Table 5 shows that the whole subunit undergoes a small rotation, somewhat larger relative to chain X (closed) than to Y (open). Of the individual helices α -12 undergoes the largest change; this is a short helix, which in the unliganded structure is in a region of weak density, just before the disordered C-terminal segment. The change in helix α -8 is the second largest, with a rotation of about 10° and a translation of over 1 Å. The movement relative to the unliganded structure is equally large for both X and Y subunits.

The four unliganded subunits resemble the open form of the liganded structure. Differences are most pronounced in helix α -8 and in strands J and K in the large domain (Figs 9 and 10); these regions have conformations that are found in neither of the liganded chains. The shift in helix α -8 is accompanied by a tilting that gives the plot (Fig. 9) a jagged appearance. In addition there are some changes throughout the large domain (left-hand side of the graph). Comparison with the closed structure shows that the shifts within the large domain mostly result from the differences between the two liganded chains, rather than differences between the liganded and unliganded structures. There are some additional changes in the effector site region of the large domain, not occurring between the two liganded structures.

The temperature factors follow roughly a similar pattern in all chains: they are plotted against residue number in Figure 11 for all subunits (liganded and unliganded), averaged over the main-chain atoms within each residue. In general the residues forming the binding sites have high *B*-factors; these residues also tend to lie between secondary structure elements. There are, however, some noticeable differences between liganded and unliganded structures. Near the C terminus the *B*-factor rises sharply in the unliganded structures (less so in chain D, which is stabilized by crystal contacts) even before the chain becomes disordered. The region involved in effector binding between α -8 and β -H (residues 210 to 215) has a considerably higher *B*-factor in the absence of ADP. The same is true for the ATP binding site, once the effect of crystal contacts in chain C is taken into account. The only region with the temperature factor consistently lower in the unliganded structures is helix α -9. This is a result of intermolecular contacts due to crystal packing along the *b*-axis. There are no apparent effects of crystal contacts on the *B*-factor in the region 277 to 279 in chains A and B. Predictably, the side-chains have higher temperature factors and show more variations while they follow similar trends to the main chain.

(d) "Consensus" structure of the unliganded enzyme

In comparisons with the liganded structure, it is confusing to consider all four independent subunits

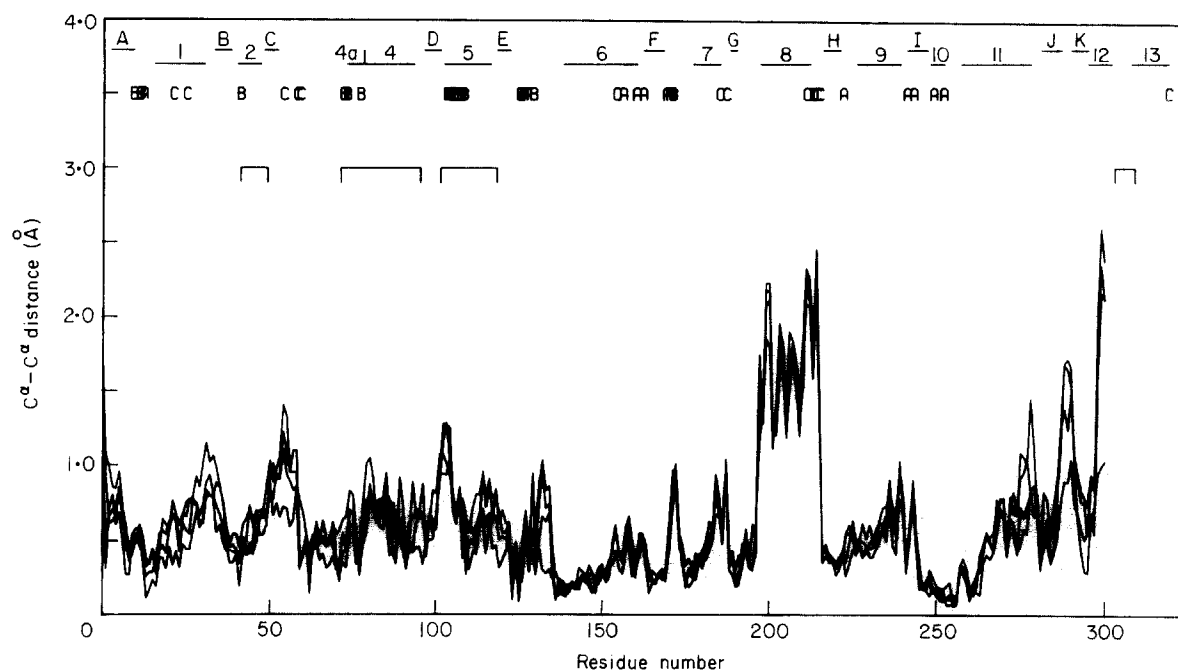


Figure 9. Shifts in co-ordinates of the α -carbons between the 4 subunits of the unliganded structure and the open subunit (Y) of the liganded structure. The shift in helix α -8 in the small domain is clearly visible. The C-terminal end of the helix forms part of the effector binding site. Tilting of the helix gives the plot its "jagged" appearance. The other large shift is near the C terminus, before it comes disordered in the unliganded structure, except in chain D, which is considerably different in that region. There are shifts of up to 1 Å spread throughout the larger domain (residues 0 to 140, 260 to 300).

of the unliganded structure, and unnecessary, provided that the differences between the crystallographically independent subunits are borne in mind. Averaging the structures would be difficult without spoiling the stereochemistry. In any case, different

parts of different subunits have to be assigned different merit; in particular, it is desirable to eliminate, as much as possible, the effects of intermolecular contacts, as these are likely to introduce local distortions to the structure (e.g. see Chothia *et*

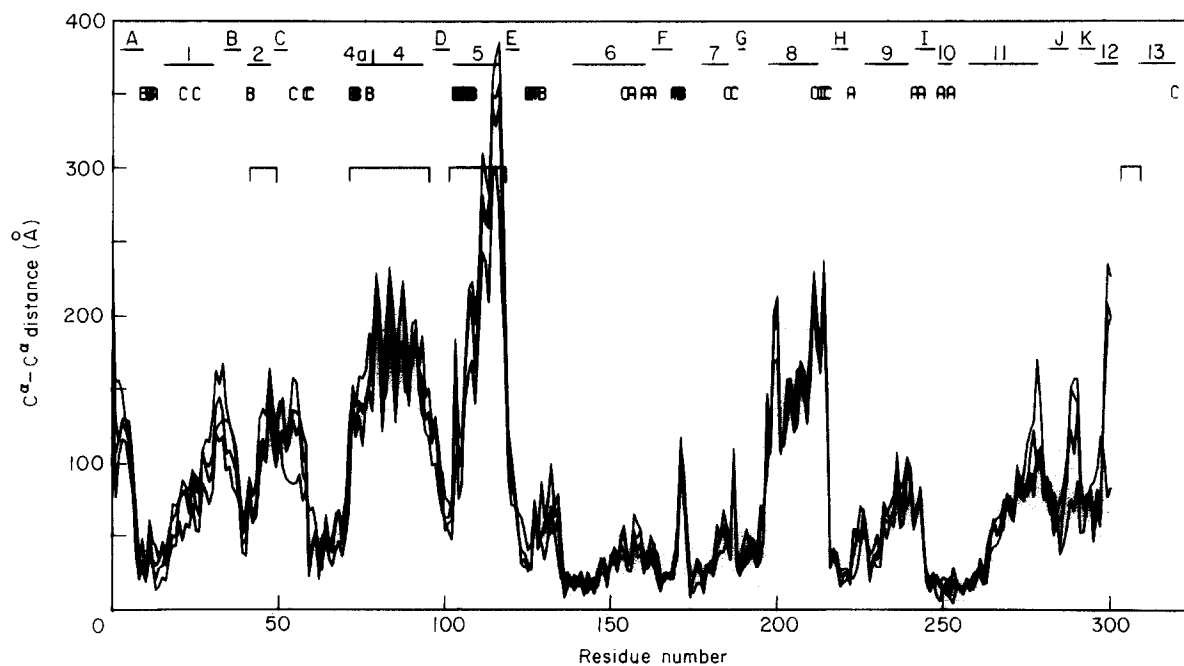


Figure 10. Shifts in co-ordinates of the α -carbons between the 4 subunits of the unliganded structure and the closed subunit (X) of the liganded structure. In the region of the small domain (140 to 260) the plot is similar to Fig. 9. The large shifts in the large domain are mostly due to closing of the active site between open and closed structures (cf. Fig. 7), although the shifts in the region between helices α -1 and β -c are now considerably larger.

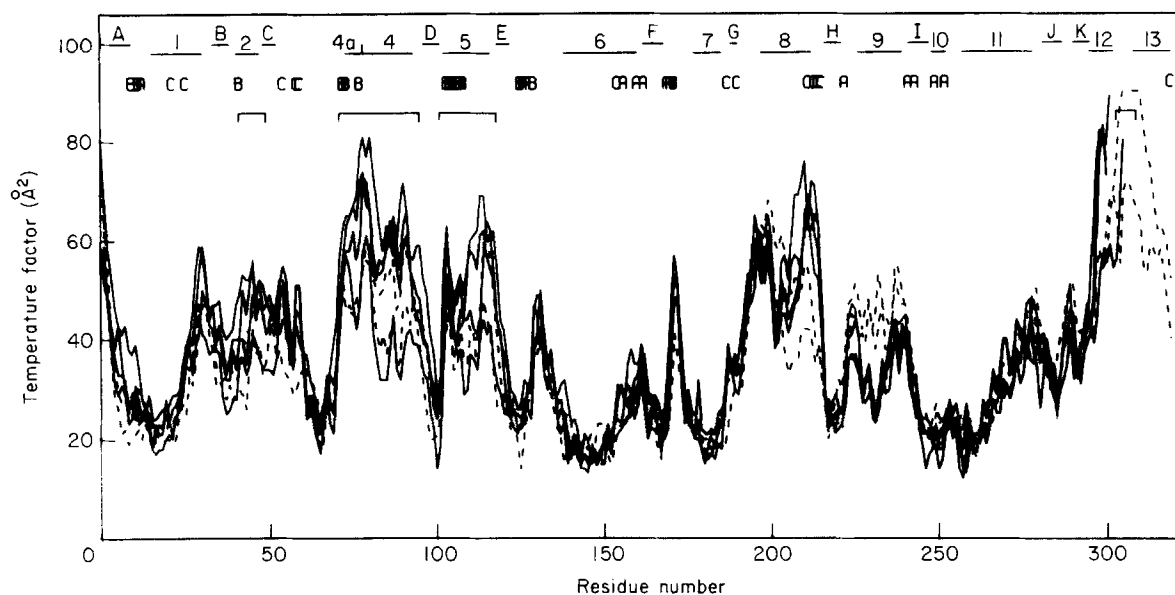


Figure 11. Temperature factors for main-chain atoms averaged over each residue for the 4 unliganded subunits (continuous lines) and the 2 liganded subunits (broken lines). The plots are roughly similar, with binding site residues tending to have high temperature factors. The C-terminal segment, which is disordered in the unliganded structure is also weak in the 2 liganded subunits, except at the C terminus itself, which is involved in binding of ADP.

et al., 1983). With this in mind a "hybrid" subunit was constructed from residues 0 to 283 of chain D and 284 to 300 of chain A. Thus the regions of crystal contacts were eliminated except for the contact around His232, which is present in all subunits. This consensus subunit is used for the following comparisons. For the purposes of comparison, all movement is considered from the liganded structure to the unliganded structure; the structures were superimposed in the molecular frame, by aligning the molecular dyad axes. Figure 12 shows the overall view of consensus subunit superimposed on the open and closed liganded chains.

(e) *The effector binding site*

Figure 13 shows a view along the long (q) axis, of one end of the molecule. Two of the effector sites

can be seen. The position of the C terminus in the liganded structure is also shown. The largest change is the shift of helix α -8 of the small domain away from the q -axis, on removal of ADP. Both the liganded structures have helix 8 in similar positions, suggesting that the shift is due only to ADP binding. A shift towards the long axis is seen in the large domains, for the unliganded structure. The shift is greater when compared with the closed structure and is consistent in direction with the closing of the active site. Although the shifts in the large domain are small, they affect a large part of the structure and are consistent in direction.

Figure 14 shows details of the effector site. The main chain of the loop at the carboxy end of helix α -8 is shifted by 2 Å away from the ADP site in the unliganded structure. This loop contains three lysine residues (211, 213 and 214), two of which (211

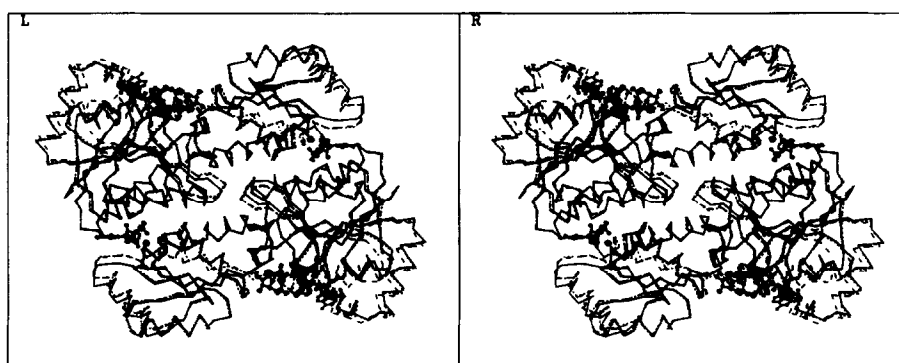


Figure 12. View along the p -axis (the same view as Fig. 1(c)) of the α -carbon trace of the unliganded structure (filled bonds) superimposed on the liganded structure (closed chain X, broken; open chain, Y, dotted) using the molecular dyad axes, showing the changes around the effector site (right and left). The only significant differences between the 2 liganded subunits are around the active site (top left and bottom right). The q -axis is horizontal, the r -axis vertical.

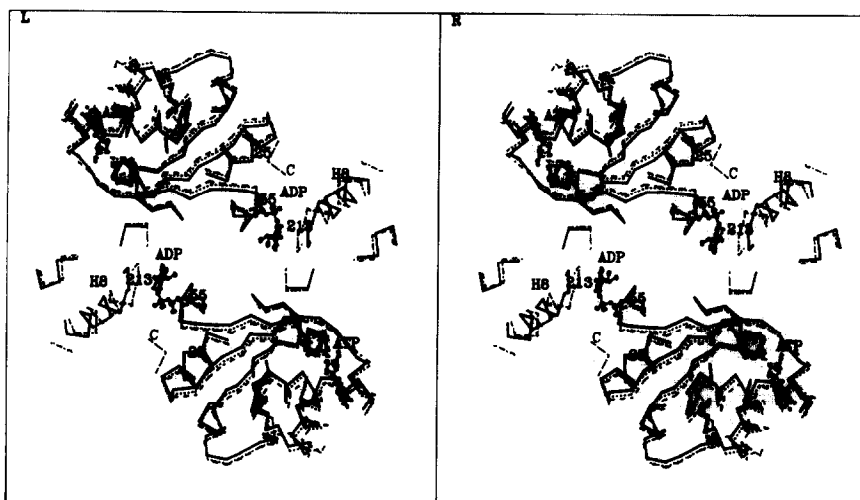


Figure 13. View down the long axis (q) of the tetramer (α -carbons), showing 2 effector binding sites. Two of the large domains are shown at the top and bottom of the drawing. Helices α -8 (small domain) are on the lower left and the upper right of the picture, labelled H8. The unliganded structure is drawn with filled bonds, the open structure is dotted and the closed structure is shown by broken lines. The motion of helix α -8 away from the centre is accompanied by a motion of the large domains towards the centre. This motion is greater in the closed subunit. The p -axis is horizontal, the r -axis vertical. Residues 25, 55, and 213 are marked for correspondence with Fig. 14.

and 214) are disordered in both structures; Lys213 is disordered in the absence of ligand in the effector site. Considerable local rearrangements accompany the overall movement of the main chain. In the non-liganded structure the guanidinium group of Arg154 is hydrogen bonded to $O\epsilon$ of Glu187. In the presence of ADP the side-chain moves 4 Å to a position where it interacts with the β -phosphate. The imidazole ring of the neighbouring His215, which in the liganded structure is involved indirectly in the binding of Mg, shifts by 3 Å in the same direction. It is stabilized there by a hydrogen bond to $O\gamma$ of Ser158. In the presence of ADP, Glu187 shifts and tilts, when its interaction with Arg154 breaks, so that its carbonyl oxygen moves by 1.5 Å away from the side-chain of Tyr319 and towards the side-chain of Phe188, which rotates through 120° about the

$C^\alpha-C^\beta$ bond, towards the side-chain of Arg204. The latter moves by 5 Å towards Tyr319. In the presence of ADP, the guanidinium group of Arg54 shifts by 4 Å to interact with the α -phosphate and the carboxy group of the now ordered C terminus. The side-chain of Arg25, which provides 2.0 to 2.5 kcal/mol (1 cal = 4.184 J) of the binding energy of both GDP and PEP (Lau & Fersht, 1987), in the absence of ligand moves into the region of the now disordered C terminus. On the other side of the intersubunit interface, the major changes include Tyr55, which is disordered or very weak in the absence of ligands. The role of this residue in binding to GDP has been recently elucidated (Lau *et al.*, 1987) by mutagenesis as being a weak (1 kcal/mol) hydrophobic contact to guanidine. The main chain of Ser58 flips 180° in the absence of

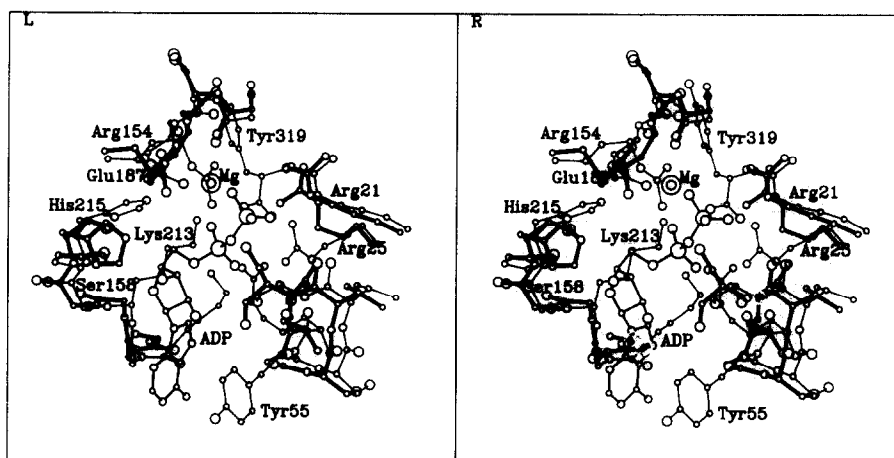


Figure 14. Details of changes in the effector binding site between unliganded (thick bonds) and liganded (thin) structures. An ADP (activator) molecule in the liganded structure is also shown. Residues from 2 different subunits are involved in binding. Residues belonging to one of the subunits are distinguished by open bonds. The double circle is the Mg ion. This view is approximately perpendicular to that in Fig. 13, roughly equidistant between the p - and r -axes.

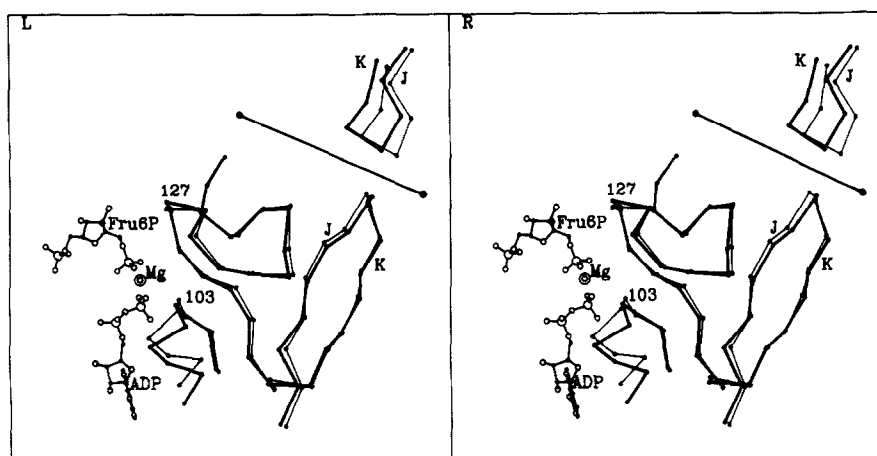


Figure 15. The β -strands J and K (on the right, around the p dyad axis, which is shown as a long line) and the catalytic loop (centre, including residue 127), showing the shift in the J-K hairpin loop. The unliganded structure is shown as thick bonds, liganded (closed, hence large change in α -5, near ADP molecule and residue 103) as thin bonds.

ADP, so the carbonyl oxygen points towards the binding site.

(f) *J-K loop*

Strands J and K of the β -sheet of the large domain form a hairpin loop that approaches its symmetry-related equivalent across the molecular p -axis. Both the liganded subunits are very similar in this region and only one (open) is shown in Figure 15. In the unliganded structure the loops formed by the strands move each by 2 Å in opposite directions, away from the coil formed by residues 125 to 138, which includes the catalytic loop of the binding site (Fig. 15). The movement results in breaking of hydrogen bonds between the coil and the β -strand J, which could weaken the structure of the catalytic part of the active site. The hydrogen bonds that break are between N of Asn288 and O δ of Asp134, O of Glu286 and N of Asp134 and between N of Glu286 and O γ of Thr133.

It is tempting to speculate that the C-terminal regions, when ordered in the presence of effectors, could in turn stabilize both the contacts between the J-K loops across the p interface and the contacts between the J β -strand and the catalytic

loop of the active site. There is, however, no direct contact between the C-terminal segment and the J and K strands, and therefore the interaction could only be indirect. That some interaction takes place is suggested by the fact that in the structure of subunit D, where the C-terminal region is partially ordered, the J-K loop is in an intermediate position between the liganded and the other unliganded structures.

(g) *The fructose-6-phosphate binding site*

It is in the binding site for the co-operative substrate Fru-6-P that we would expect to see substantial differences in the T-state conformation, to explain its low affinity for Fru-6-P. Surprisingly, this site is little changed from that in the liganded structure (Fig. 16). All the groups that interact with Fru-6-P seem to be more or less in their binding positions, and many of them are not even less well ordered. The main difference in the Fru-6-P site is in the loop containing Arg171, between β -F and α -7. Arg171 has a minor effect in stabilizing the negative charge on the transition state (Hellinga & Evans, 1987). In the liganded structures the loop forms a tight β -turn with O of Gly170 hydrogen bonded to

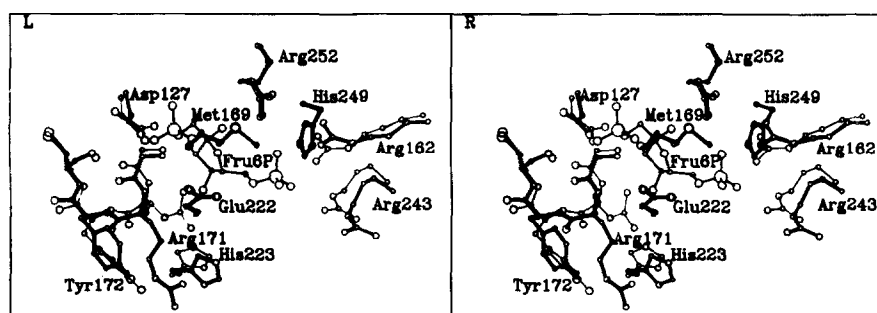


Figure 16. Fru-6-P binding site, showing only minor changes from the liganded structure. The β -bend discussed in the text (residues 170 to 173) is shown on the left. The unliganded structure is shown as thick bonds, the liganded as thin bonds. Residues 162 and 243 (open bonds) belong to a different subunit. The view is approximately along the q -axis, with p near horizontal and r vertical.

N of Cys173. Arg171 is in a poor Ramachandran region with the side-chain pointing towards the γ -phosphate of ATP. In the absence of ligand, the β -turn twists and the peptide plane of Gly170 flips by 60° so that, while the hydrogen bonding is preserved, the carbonyl oxygen points out of the plane of the β -turn by about 30° on the other side. The main chain of Tyr172 tilts by 45° . Arg171 is now in a better Ramachandran region, with its side-chain pointing away from the binding site, between the side-chains of His223 and Tyr172 that had moved to accommodate it. As well as this change, there is some disordering in Arg162 and Arg243, which bind the 6-phosphate from the other subunit; Arg243 also moves about 2 \AA away from the binding site. The changes do not seem to be large enough to account for a major difference in affinity.

(h) The ATP binding site

Although the large domain in the unliganded structure is generally more similar to the open than to the closed liganded subunit, in the ATP binding site itself, the unliganded structure is intermediate between the two liganded structures (Fig. 17). Most of the side-chains that interact with ADP become less ordered: in particular, arginines 72 and 77 are disordered or very weak in the absence of ligand, consistent with their role in binding.

4. Discussion

The relationship between a protein conformation seen in a crystal and that occurring in solution is always difficult to assess, particularly in an allosteric protein, which has essential conformational flexibility. These crystals were grown from solutions that would be expected to contain the low-affinity T-state conformation of PFKase, i.e. in the absence of any activating ligands (Fru-6-P, ADP or P_i). Crystals could also be grown with the inhibitor 2-phosphoglycolate, but even in the absence of inhibitor, the T-state should be predominant ($L_0 =$

$[T]/[R] = 4 \times 10^6$; Blangy *et al.*, 1968). Yet compared to the active conformation, the unliganded structure does not show the substantial quaternary structure change seen in the *B. stearrowthermophilus* PFKase T-state structure (Evans *et al.*, 1986). Moreover, the active site shows few changes, and it is hard to see why Fru-6-P could not bind easily. Indeed, preliminary results show that Fru-6-P can be bound in the active site in the crystals, without causing significant conformational changes (T. Schirmer, unpublished results). Such changes as there are radiate out from the effector site, and seem to be a result of the lack of a ligand there, permitting the opening of that site, and the disordering of the C terminus. This structure thus seems to be a conformation that would have a high affinity for substrate Fru-6-P, rather than the expected low affinity. Two questions then arise: (1) to what conformation in solution does this structure correspond; and (2) if it is not the T-state, why have we not crystallized what should be the main species in solution?

The changes seen in this structure relative to the liganded conformation can be considered as starting at the effector site. When the activator ADP is removed, the site opens up, the small domains move away from the q -axis (helix α -8 and loop 211 to 215), and the large domains move towards the q -axis (Fig. 13). The C-terminal region (residues 301 to 319, including helix α -13) becomes disordered, and this may indirectly cause the movement of the J-K hairpin loop, which is near the catalytic site. The movement is quite large around the effector site (up to $\sim 2 \text{ \AA}$), but is attenuated to small changes around the active site.

The disordering of the C terminus when no ligand is bound in the effector site is consistent with the observation that either GDP or PEP protect the enzyme against proteolysis; Le Bras & Garel (1982) showed that 40 to 50 residues could be removed from the C terminus of the unliganded enzyme, and that this truncated derivative has reduced co-

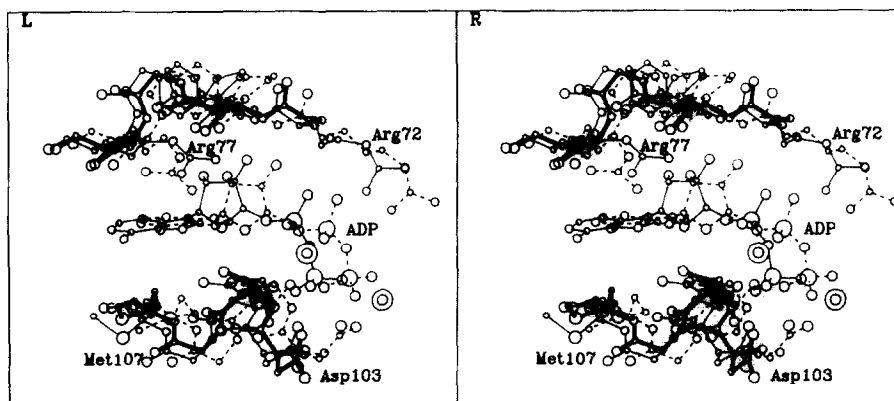


Figure 17. View into the ATP/ADP substrate site, from a point approximately equidistant from all molecular axes. Three structures are superimposed: unliganded (thick bonds), open (thin bonds) and closed (broken bonds). The side-chains of Arg72 and Arg77 are disordered in the unliganded structure. The product molecules (ADP) are shown for the liganded structures: the double circles are Mg ions.

operativity, and dissociates more readily into dimers. They describe the C terminus as a covalently bound allosteric effector, which makes the tetramer more stable and more co-operative.

If this structure does not represent a low-affinity state, what is it? One possibility is that it corresponds to the conformation of the enzyme when activated by substrate Fru-6-P, but not by the heterotropic activator ADP (or GDP). The other crystal structures of PFKase have all had a ligand in the effector site, an activating ligand (ADP or P_i) in the case of the R-state structures, or an inhibitor (2-phosphoglycolate) in the case of the *B. stearothermophilus* T-state structure. This could explain the observation in this study of substantial changes centred on the effector site.

Why do these crystals not contain a low-affinity conformation? The precipitating agent polyethylene glycol does not seem to affect the kinetics up to 10% concentration (C. E. Kundrot, unpublished results), so an activating effect of the crystallization medium is unlikely, although the effect of 1 M-NaCl has not been investigated. There is no evidence in the electron density maps of unexpected ligands (e.g. substrates or phosphate ions) in any of the binding sites. The alternative explanation is that the crystallization process has selected the less-common conformation from solution, either because the crystal forces are sufficient to compensate for the difference in energy between the conformations, or because the minor component is selected kinetically once the crystals start growing. It may be significant that this crystal form grows rarely unless seeded with previously grown nuclei. Both types of tetramer in the crystal (i.e. (AB)₂ and (CD)₂) have similar packing interactions in one direction, along the crystal *y*-axis, and this contact involves the outer layer of the small domain (particularly helix α -9), which changes its conformation in the T to R-state transition. It is possible that this crystal contact accounts for both the independent tetramers having the same unexpected conformation.

The co-ordinates and diffraction data have been deposited with the Protein Data Bank, Chemistry Department, Brookhaven National Laboratory, Upton NY 11973, U.S.A., from whom copies are available. W.R.R. was supported by an MRC studentship. We thank the staff of the Daresbury Synchrotron Radiation Facility for their assistance in data collection.

References

- Blangy, D., Buc, H. & Monod, J. (1968). *J. Mol. Biol.* **31**, 13–35.
- Bricogne, G. (1976). *Acta Crystallogr. sect. A*, **32**, 832–847.
- Buehner, M., Hecht, H.-J., Hensel, R. & Mayr, U. (1982). *J. Mol. Biol.* **162**, 819–838.
- Cass, K. H. & Stellwagen, E. (1975). *Arch. Biochem. Biophys.* **171**, 682–684.
- Chothia, C., Lesk, A. M., Dodson, G. G. & Hodgkin, D. C. (1983). *Nature (London)*, **302**, 500–505.
- Crowther, R. A. (1972). In *Molecular Replacement Method* (Rossmann, M. G., ed.), pp. 173–178. Gordon and Breach, New York.
- Evans, P. R. & Hudson, P. J. (1979). *Nature (London)*, **279**, 500–504.
- Evans, P. R., Farrants, G. W. & Hudson, P. J. (1981). *Phil. Trans. Roy. Soc. ser. B*, **293**, 53–62.
- Evans, P. R., Farrants, G. W. & Lawrence, M. C. (1986). *J. Mol. Biol.* **191**, 713–720.
- Fermi, G., Perutz, M. F., Shaanan, B. & Fourme, R. (1984). *J. Mol. Biol.* **175**, 159–174.
- Fox, G. C. & Holmes, K. C. (1966). *Acta Crystallogr.* **20**, 886–891.
- French, G. S. & Wilson, K. (1978). *Acta Crystallogr. sect. A*, **34**, 517–525.
- Hellings, H. W. & Evans, P. R. (1987). *Nature (London)*, **327**, 437–439.
- Hengartner, H. & Harris, J. I. (1975). *FEBS Letters*, **55**, 282–285.
- Herzberg, O. & Sussman, J. L. (1983). *J. Appl. Crystallogr.* **16**, 144–150.
- Jack, A. & Levitt, M. (1978). *Acta Crystallogr. sect. A*, **34**, 931–935.
- Jones, T. A. (1978). *J. Appl. Crystallogr.* **11**, 268–272.
- Konnert, J. H. (1976). *Acta Crystallogr. sect. A*, **32**, 614–617.
- Konnert, J. H. & Hendrickson, W. A. (1980). *Acta Crystallogr. sect. A*, **36**, 344–350.
- Lau, F. T.-K. & Fersht, A. R. (1987). *Nature (London)*, **325**, 811–812.
- Lau, F. T.-K., Fersht, A. R., Hellings, H. W. & Evans, P. R. (1987). *Biochemistry*, **26**, 4143–4148.
- Le Bras, G. & Garel, J.-R. (1982). *Biochemistry*, **21**, 6656–6660.
- Matthews, B. W. (1968). *J. Mol. Biol.* **33**, 491–498.
- Monod, J., Wyman, J. & Changeux, J.-P. (1965). *J. Mol. Biol.* **12**, 88–118.
- Nixon, P. E. & North, A. C. T. (1976). *Acta Crystallogr. sect. A*, **32**, 320–325.
- North, A. C. T., Phillips, D. C. & Mathews, F. S. (1968). *Acta Crystallogr. sect. A*, **24**, 351–359.
- Oatley, S. & French, S. (1982). *Acta Crystallogr. sect. A*, **38**, 537–549.
- Phillips, S. E. V. (1980). *J. Mol. Biol.* **142**, 531–554.
- Rubin, M. M. & Changeux, J.-P. (1966). *J. Mol. Biol.* **21**, 265–274.
- Schutt, C. & Winkler, F. K. (1977). In *The Rotation Method in Crystallography* (Arndt, U. W. & Wonacott, A. J., eds), pp. 173–186. North Holland, Amsterdam.
- Shirakihara, Y. & Evans, P. R. (1988). *J. Mol. Biol.* **204**, 973–994.
- Sussman, J. L., Holbrook, S. R., Church, G. M. & Kim, S.-H. (1977). *Acta Crystallogr. sect. A*, **33**, 800–804.
- Tanaka, I., Appelt, K., Dijk, J., White, S. W. & Wilson, K. S. (1984). *Nature (London)*, **310**, 376–381.
- Winkler, F. K., Schutt, C. & Harrison, S. C. (1979). *Acta Crystallogr. sect. A*, **35**, 901–911.